Earth Systems and Climate Change Hub

National Environmental Science Programme

ACCESS Climate model simulations for the Coupled Model Intercomparison Project (CMIP6)

Rashid HA, Dix M, Sullivan A, Bodman R, Zhu HY

July 2020

Earth Systems and Climate Change Hub Report No. 14

Australian Government

National Environmental Science Programme

The Earth Systems and Climate Change Hub is supported by funding through the Australian Government's National Environmental Science Program. The Hub is hosted by the Commonwealth Scientific and Industrial Research Organisation (CSIRO), and is a partnership CSIRO, Bureau of Meteorology, Australian National University, Monash University, University of Melbourne, University of New South Wales and University of Tasmania. The role of the Hub is to ensure that Australia's policies and management decisions are effectively informed by Earth systems and climate change science, now and into the future. For more information visit www.nespclimate.com.au.

Citation

Rashid HA, Dix M, Sullivan A, Bodman R, Zhu HY. 2020. *ACCESS climate model simulations for the Coupled Model Intercomparison Project (CMIP6)* Earth Systems and Climate Change Hub Report No. 14. Earth Systems and Climate Change Hub, Australia.

Contact

Enquiries regarding this report should be addressed to:

Harun Rashid

CSIRO

harun.rashid@csiro.au

July 2020

This report is available for download from the Earth Systems and Climate Change Hub website at www.nespclimate.com.au.

Contents

1 Introduction 6
2 Results 8
2.1 Surface temperatures 8
2.2 Interannual climate variability 11
2.3 Rainfall simulation by a higher-resolution ACCESS-AM 15
3 Conclusions 18
4 Acknowledgements 20
5 References 20

Figures

Figure 1. Observed and model simulated GMST evolutions over the historical period (1850-2014), and the future model projections for different scenarios (2015-2100). 9

Figure 2. Systematic errors or biases (in degrees Celsius) of model simulated ensemble-mean SSTs with respect to the observed SST over the period 1900-2014. .10

Figure 3. Zonal profiles of time and meridional mean SST, zonal wind stress and thermocline depth (left column) and of the anomalous variations of these variables (right column). 12

Figure 4. Spatial structures of ENSO, as represented by the dominant EOFs of tropical Pacific SST 13

Figure 5. Annual variations of the standard deviations of ENSO-related SST anomalies (in degrees Celsius, left panel), and the power spectra (right panel) for observation (black curve) and model simulations (coloured curves). 14

Figure 6. Cross correlations between the Niño-3 SST index and the Niño-3.4 D20 index as a function of time lag. The SST index leads at positive lags and the D20 index leads at negative lags. The Niño-3.4 D20 index is used as a proxy for zonally averaged thermocline depth anomalies, which in turn are an indication of the upper-ocean heat content in the tropical Pacific. 15

Figure 7. (a) Annual mean rainfall rate in mm/day for the ACCESS-AM control experiment; (b) Annual mean rainfall bias (mm/day) with respect to the GPCP rainfall observations (1989-2014). 16

Figure 8. The difference of the annual mean rainfall rates (mm/day) between the experiment with 60 km resolution and the control experiment (135 km) for 1989-2014. 17

Figure 9. The difference of the annual mean rainfall rates (mm/day) between the model experiment with improved convection scheme and the control experiment. (1989-2014). 17

REPORT SUMMARY

Reliable climate change information is crucial for better informed policy development and decision-making outcomes for the Australian Government and other stakeholders, including next and end-users.

In preparation for the World Climate Research Programme's Coupled Model Intercomparison Project (CMIP) sixth phase, the previous ESCC Hub *Project 2.1: Preparing ACCESS for CMIP6* updated Australia's national climate model, the Australian Community Climate and Earth System Simulator (ACCESS). For submission to CMIP6, climate models are required to complete a series of mandatory experiments designed to meet CMIP6 protocol (Eyring et al., 2016). These standardised experiments allow climate models, including ACCESS, to be benchmarked against simulations from other global climate models.

The current Hub *Project 5.1: ACCESS evaluation and application* builds on the simulations submitted to CMIP6 by completing an ensemble of simulations using the coupled and atmospheric model versions of ACCESS (ACCESS-CM and ACCESS-AM), as well as the Earth Systems Model (ACCESS-ESM1.5), which incorporates the carbon cycle.

These ACCESS simulations have been submitted to the CMIP6 archive and will be accessed and utilised by researchers worldwide to produce peer-reviewed publications that will inform the Intergovernmental Panel on Climate Change (IPCC) Sixth Assessment Report. Additional ensembles have also been completed which will provide underpinning data for Australian researchers to further investigate the effects of human-induced greenhouse gas emissions on climate drivers that influence Australia's weather and climate, such as the El Niño–Southern Oscillation, the Southern Annular Mode and the Indian Ocean Dipole, and how they may change in the future under a warming climate.

This report describes the performance of two ACCESS models (ACCESS-CM2 and ACCESS-ESM1.5) in realistically simulating some key climate variables over the historical period (1850-2014). Both models show good accuracy over the historical period, giving additional confidence to the ability of ACCESS models to accurately project the future climate.

This report also includes preliminary analysis of the ensemble simulations for up to the year 2100, and notes that ACCESS-CM2 projects a warmer global mean surface temperature at year 2100 (up to 6 degrees warmer than present days) owing to a higher climate sensitivity, the reasons for which are yet to be investigated. The performance of ACCESS-CM2 in simulating the ENSO was also analysed, with results showing that the models simulate the key features reasonably well, although further effort is needed to continue to improve the simulation of ENSO in the ACCESS model.

1 Introduction

A key objective of the ESCC Hub Project 5.1 is to generate an ensemble (multiple model runs) of climate simulations by two versions of the ACCESS (Australian Community Climate and Earth System Simulator) model, ACCESS-CM2 and ACCESS-ESM1.5. This ensemble will supplement the single-member ACCESS simulations already contributed to the international Coupled Model Intercomparison Project Phase 6 (CMIP6). The ensemble of simulations will allow for, among other things, a better estimate of climate change signals associated with anthropogenic greenhouse gas and aerosol forcings. They also provide confidence limits for uncertainty arising from the unforced internal climate variability.

These simulations, spanning the historical period (1850-2014) and future projection period (2015-2100), are expected to underpin some of the research being undertaken by other ESCC (Earth System and Climate Change) Hub projects. Researchers are presented with opportunities to analyse these ensemble simulations to investigate various scientific questions relating to Australian as well as global climate.

In this report, we describe some aspects of simulations by ACCESS-CM2 and ACCESS-ESM1.5 and the multi-decadal runs from ACCESS-AM (the atmospheric component of ACCESS-CM2) with two different horizontal resolutions and an updated convection scheme. In particular, some of the simulated climate variables (e.g., surface temperatures, rainfall, the zonal winds and upper-ocean heat content) are analysed and compared with observations. The purpose of this report is to:

- Document how realistically the two ACCESS models simulate the main climate variables over the historical period (for which observations are available)
- Have a preliminary look at the projected climate
- Examine the atmosphere-ocean coupled variability associated with an important climate variability mode, namely, El Niño–Southern Oscillation (ENSO), and
- Compare the rainfall simulation performance of a higher-resolution ACCESS-AM with that of two lower-resolution versions of the model with and without improved convection physics.Models and data

Under Hub project 5.1, we used data from various coupled simulations of ACCESS-CM2 and ESM1.5 models and atmosphere-only simulations of ACCESS-AM with N96 and N216 horizontal resolutions (~ 135 km and 60 km grid spacing, respectively). The coupled experiments were designed following the CMIP6 protocol (Eyring et al., 2016), with prescribed climate radiative forcings arising from anthropogenic greenhouse gas and aerosol concentrations. The latter derive from observational estimates over the historical period and from future scenarios based on a matrix of shared socioeconomic pathways (SSPs). The data used in this study are from multiple historical and scenarioMIP simulations of ACCESS-CM2 and ESM1.5. A complete description of ACCESS model configurations and the CMIP6 simulations are found in Bi et al. (2020) and Ziehn et al. (2020).

The atmosphere-only simulations were performed using the AMIP (Atmospheric Model Intercomparison Project) protocol (Gates et al., 1999), in which the atmospheric model is run with prescribed observed monthly and interannually varying sea surface temperature

and sea ice extent. Two 26-year (1989-2014) AMIP simulations were performed using an experimental version of ACCESS-AM, after configuring the model to have different horizontal resolutions (N96 and N216) but the same vertical resolution, with 85 levels extending from surface to a height of about 85 km. Other multiple AMIP simulations with the same N96 horizontal resolution have also been completed, which are described in Bodman et al, 2020. We have not used these single-resolution AMIP runs in this report, as an objective here is to compare the reductions of rainfall error due to increasing model resolution and an improvement in the model's convection physics. The atmospheric model incorporates a comprehensive set of sophisticated physical parameterization schemes, including the radiation, convection, cloud, atmospheric boundary layer, gravity wave drag, atmospheric aerosols and chemistry, and land surface and hydrology schemes. A detailed description of these processes is given in a recent publication (Walters et al., 2019). One extra AMIP simulation was also carried out, in which the deep convective entrainment rate was allowed to vary over a realistic range of values by linking it to the amount of convective activity within the last several hours. This is the key improvement of the Global Atmosphere version 8 (GA8) model physics in UM. The GA8 version is due to be released later this year (by the UK Met Office) and will be widely used in ACCESS communities, including Bureau of Meteorology, CSIRO and Australian universities. Evaluation of the GA8 model package has been an important part of collaboration with UK Met office.

To compare the models' initial results, we use observational and reanalysis datasets including the Hadley Centre and the Climatic Research Unit dataset (HadCRUT4), the Global Precipitation Climatology Project (GPCP) version 2.2 (Adler et al. 2003), HadISST (Rayner et al., 2003), ERA-40/ERA-Interim (Dee et al., 2011; Uppala et al., 2005) and the Australian Bureau of Meteorology's POAMA Ensemble Ocean Data Assimilation System (PEODAS) dataset (Yin et al., 2011). Time and area averages, as well as anomalies with respect to climatological annual cycles were used. The SST anomalies were subjected to empirical orthogonal function (EOF) analysis over the tropical Pacific domain (130E-80W, 20S-20N) to investigate the dominant mode of interannual climate variability (i.e., ENSO).

2 Results

2.1 Surface temperatures

The global mean surface temperature (GMST), which is the area-weighted average of near-surface air temperatures, is often used as a primary indicator of global climate variability and change. The anomalies of GMST from ACCESS-CM2 and ACCESS-ESM1.5 are compared with those from the HadCRUT4 dataset in Fig. 1. The anomalies in this case were computed with respect to the 1960-1990 time means (hence, the closer match between observations and simulations during that period). The temporal evolution of ensemble mean GMSTs from the two models compares well with the observed GMST evolution (Fig. 1, top left), which shows a general warming trend with weak (or even negative) and accelerated warming periods. The modelled GMST anomalies, however, tend to be around 0.2˚C warmer than observed during the earlier periods of historical simulation. After about 2000, the simulated anomalies are also warmer than the observed GMST, partly because of the absence of the recently observed warming pause in climate models. This discrepancy between model simulations and observation are commonly seen in the CMIP class models and has been the subject of many studies (Kosaka & Xie, 2013; Risbey et al., 2014). One of the proposed explanations is that the observed pause is a result of modulation of the GHG induced warming trend by a La-Niña-like decadal cooling in the tropical eastern Pacific. Such decadal coolings do exist in model simulations; however, being the result of unforced natural variability, they may not be necessarily in phase with the observed cooling (which temporarily arrests the warming trend), giving rise to the discrepancy mentioned above. There is also a period of prolonged cooling in the mid-twentieth century, which both models simulate well. This interdecadal cooling trend was strongly influenced by the cooling effect of anthropogenic aerosol forcing (Wilcox et al., 2013). Additionally, there are short global cooling periods caused by strong volcanic eruptions throughout the 19th and 20th centuries (e.g., 1883, 1902, 1963, 1982, 1991). These are harder to see as there are also warming and cooling periods resulting from considerable natural climate variability.

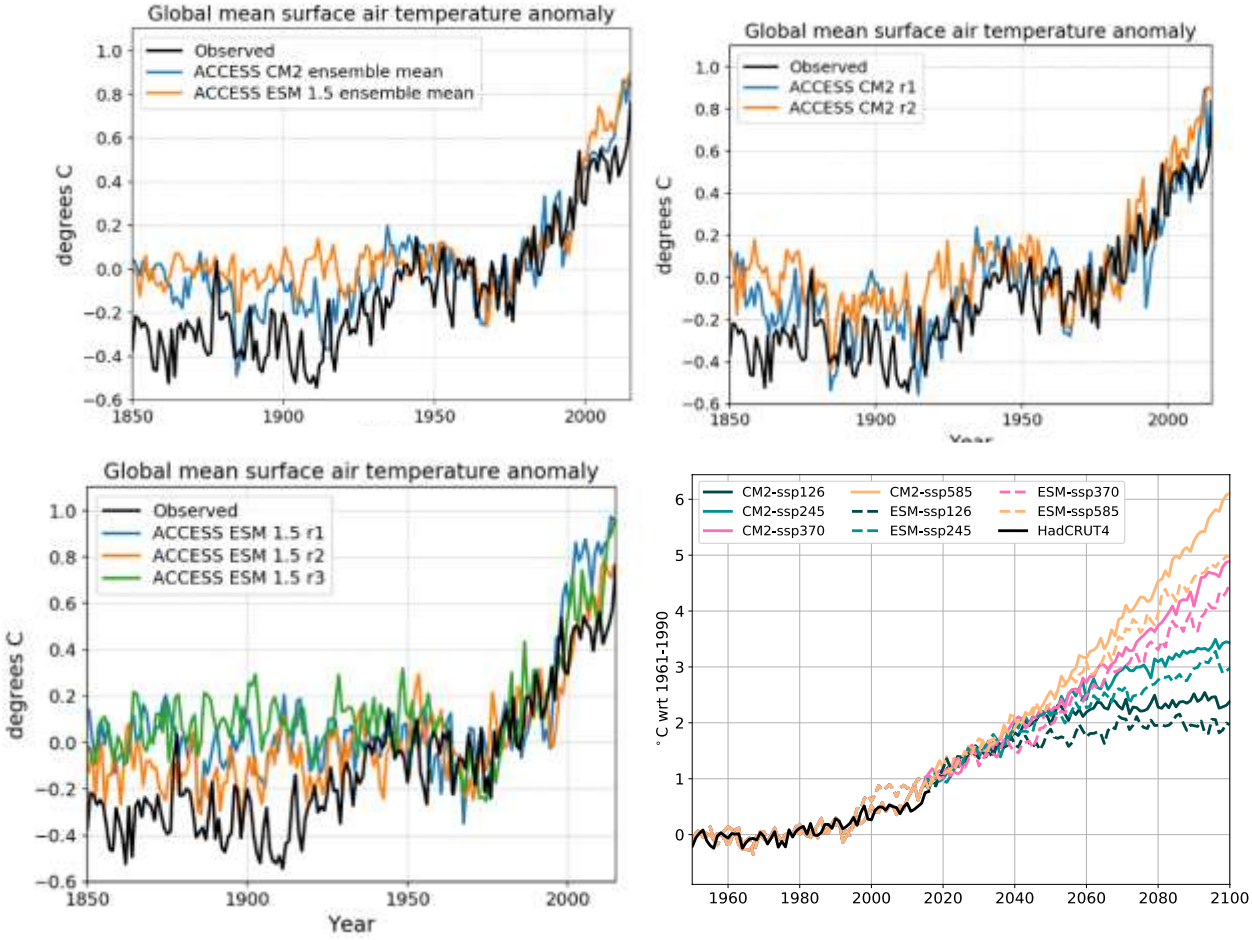

Figure 1. Observed and model simulated GMST evolutions over the historical period (1850-2014), and the future model projections for different scenarios (2015-2100). Top left: Observed and simulated ensemble mean GMSTs. Top right: Observed GMST and the individual simulations from ACCESS-CM2; bottom left: Observed GMST and the individual simulations from ACCESS-ESM1.5. Bottom right: Future projections of GMST from ACCESS-CM2 and ACCESS-ESM1.5 under various scenarios (also included is a portion of historical GMST data for 1950-2014).

The latter is, however, more pronounced in individual ensemble members of ACCESS-CM2 and ACCESS-ESM1.5 simulations (top right and bottom left panels of Fig. 1, respectively) than in the corresponding ensemble means (top left panel). In the remaining panel of Fig. 1 (bottom right), the projected GMSTs for four future scenarios, namely the shared socioeconomic pathways (SSPs) 126, 245, 370 and 585, are shown for up to the year 2100. The solid lines indicate the ACCESS-CM2 projections and the dashed lines the ACCESS-ESM1.5 projections. The models project GMSTs that are up to six degrees higher than the 1960-1990 mean GMST. The CM2 projected GMSTs are somewhat higher than those from ESM1.5, because the former model has a higher equilibrium climate sensitivity (i.e., the increase in GMST due to a doubling of CO_2 concentration) than the latter.

The sea-surface temperature (SST) is another important climate variable that affects (atmospheric) day-to-day weather, as well as low-frequency climate variability. Improving the realism of SST simulation has been a key focus of ACCESS model development. The systematic errors (or biases) in simulated historical SSTs are shown in Fig. 2. The biases were estimated by first calculating the ensemble mean of the time-mean SSTs from individual members and then subtracting the observed time-mean SST from the ensemble mean, for a time period of 1900-2014. The SST bias for ACCESS-CM2 (top panel of Fig.

2) shows an overall warm bias in the Southern Hemisphere (SH) and a cold bias in the Northern Hemisphere (NH). The warm bias is large over the Southern Ocean (SO), except for the Pacific sector, and adjacent to the west coasts of South America and Africa. The cold biases are prominent in the Northern Pacific Ocean and Atlantic Ocean, especially near the western boundary currents. The spatial pattern of the bias in historical SST simulation is similar to the bias pattern for the pre-industrial SSTs (the spin-up phase; Bi et al. 2020), although the simulated historical SSTs tend to be slightly colder, especially in NH. ACCESS-ESM1.5 (bottom panel) shows predominantly warm biases over most of the global oceans, except for a few areas near the tropical Pacific and Atlantic Oceans and near the Asian continental coasts. The warm bias is again large and widespread over SO. The dominance of warm bias in ACCESS-ESM1.5 is consistent with its higher GMST seen in Fig. 1.

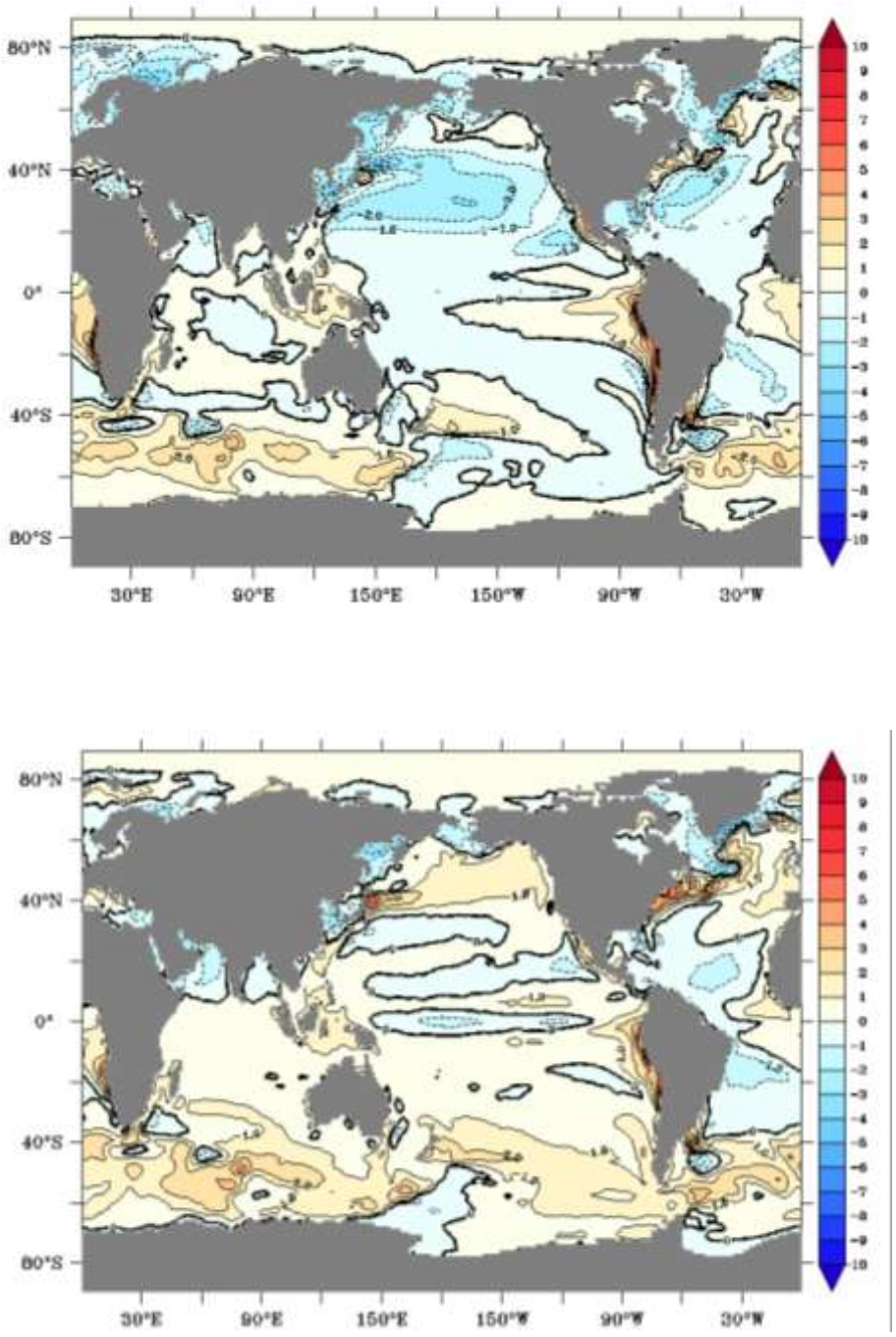

Figure 2. Systematic errors or biases (in degrees Celsius) of model simulated ensemble-mean SSTs with respect to the observed SST over the period 1900-2014. ACCESS-CM2 model bias is shown on the top panel and ACCESS ESM1.5 model bias is shown on the bottom panel.

2.2 Interannual climate variability

In addition to climate change, an important use of climate models is to study interannual (i.e., year-to-year) climate variability. Australia, like many other countries, experiences signicant interannual variations in its climate. Therefore, an important goal of ACCESS model development has been to simulate interannual variability that compares favourably with observations. There are different modes of interannual variability in nature; the most prominent of which is El Niño–Southern Oscillation (ENSO). This mode originates in the tropical Pacific as a result of air-sea interactions and profoundly influences the weather and climate of various parts of the globe. Here, we examine how realistically ACCESS-CM2 simulates this important mode of climate variability. The performance of ENSO simulation in precursor coupled version of ACCESS-ESM1.5 (i.e., ACCESS1.3) was documented elsewhere (Rashid et al., 2013).

The time-mean state of the tropical Pacific Ocean is important for ENSO simulation. We show in Fig. 3 the time means (left column) and standard deviations (right column) of the meridionally-averaged (over 5S–5N) SST, zonal wind stress (Taux) and the thermocline depth (D20, approximated as the depth of 20˚C isotherm). These three variables mutually interact to determine bulk of the ENSO properties. Data are plotted from observations (black curve) and two ACCESS-CM2 historical simulations (red and blue curves) and one pre-industrial control simulation (green curve). The simulated data are broadly similar to observations. The mean SSTs are warmer in the western Pacific than in the eastern Pacific, both in observation and simulations. However, the simulated SSTs are cooler than the observed SST in the western and central Pacific and warmer in the far eastern Pacific, depicting a reduced east-west SST gradient (top-left panel of Fig. 3). Consistent with the latter, the mean zonal wind stress, which is related to the easterly trade winds over the tropical Pacific, is weaker than the observed (i.e., reanalysed) zonal wind stress over the central and eastern equatorial Pacific, but stronger over west of the dateline (middle-left panel). Additionally, the thermocline depth is shallower than observed over the western and central Pacific (bottom-left panel). There are hardly any differences in the time-mean quantities from two historical and one pre-industrial control simulations. These ACCESS-CM2 biases in the tropical Pacific mean climate (as represented by SST, zonal wind stress and thermocline depth) are consistent with each other and result from dynamical interactions involving these three variables. For example, a weaker easterly trade wind leads to a smaller SST gradient (due to less warm SSTs over the western and central equatorial Pacific) and a flatter thermocline; in turn, the smaller SST gradient leads to weaker easterly winds, thus completing a feedback loop.

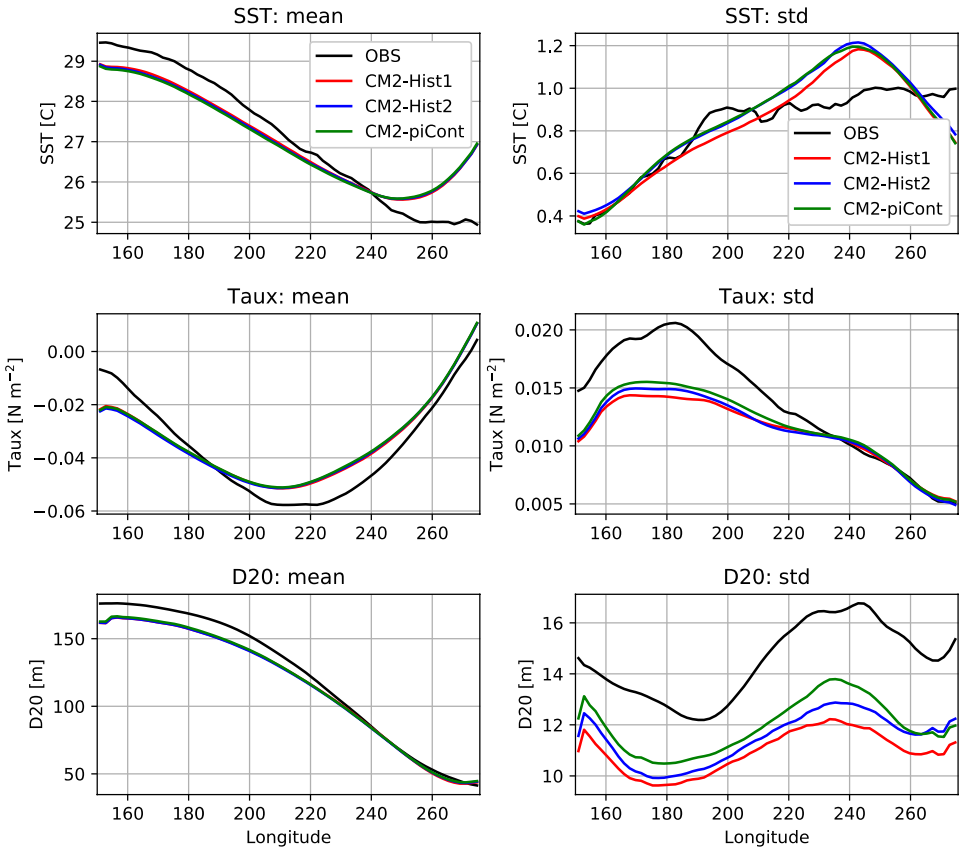

Figure 3. Zonal profiles of time and meridional mean SST, zonal wind stress and thermocline depth (left column) and of the anomalous variations of these variables (right column).

The anomalous (i.e., non-seasonal) variation of SST is the lowest in the western Pacific and highest in the eastern Pacific; the observations and model simulations again broadly agree with each other (top-right panel). The highest SST variability in the eastern Pacific is associated with the ENSO phenomenon, which makes the SSTs in the central to eastern Pacific become anomalously warm and cold by several degrees during its opposite phases. The model-simulated SST variability is found to be stronger than the observed variability, especially in the eastern Pacific. There are also some differences between the model simulations, although these are not as large as their differences with the observation. For zonal wind stress, the observed and simulated anomalous variations become gradually stronger going from the eastern to the central and western Pacific; however, in the latter regions, the model simulates much weaker variability than in observation (middle-right panel). For thermocline depth, the observed anomalous variability is a minimum to the east of the dateline and increases farther east. The simulated variability has a similar pattern, but this is lower than the observed variability throughout the equatorial Pacific (bottom-right panel).

The latitude-longitude patterns of the above anomalous variability, decomposed into the modes of variability, are of interest, as these patterns reveal the horizontal structure of ENSO in the tropical Pacific. The patterns and their time evolutions were obtained by an empirical orthogonal function (EOF) analysis of SST anomalies. Fig. 4 shows the spatial structures of three most dominant modes (according to the explained variances) in three rows. The observed structures (the left-most column) show the centres of high SST variability, which may be in phase (shown by the same colour shading) or in opposite phases (contrasting colour shadings). For the first mode (top-left), which explains more

than half of the total observed SST variability, the highest variability is located in the tropical eastern and central Pacific along the equator. The three ACCESS-CM2 simulations (columns 2-4) show a similar pattern, but the meridional extent of the patterns

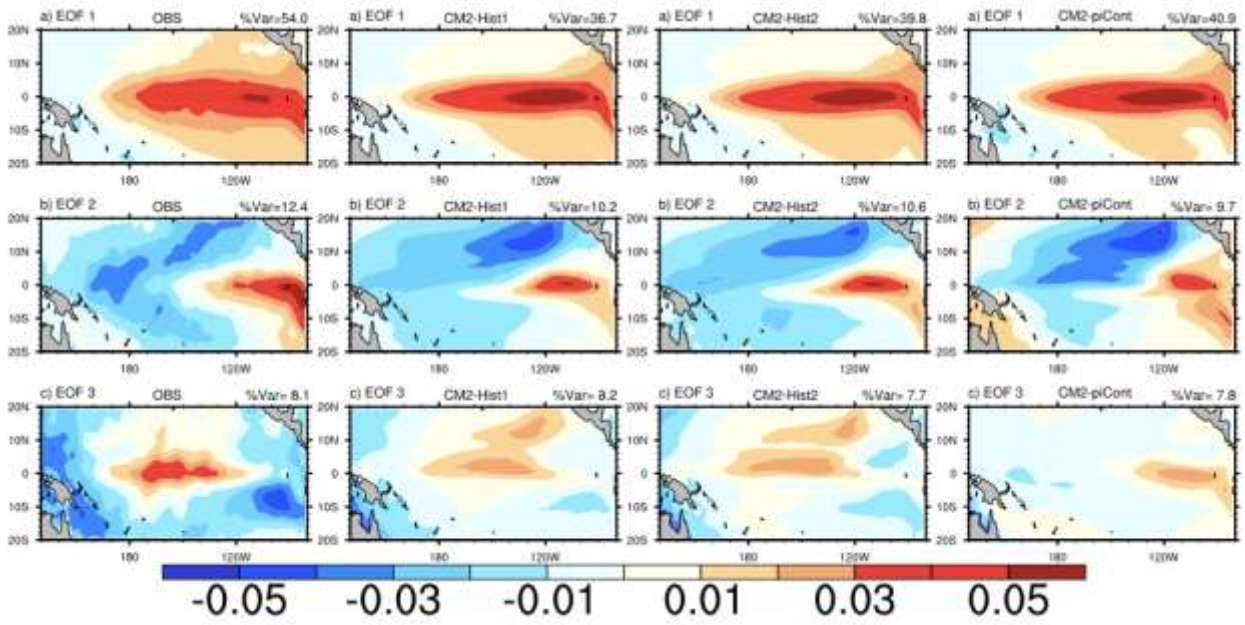

Figure 4. Spatial structures of ENSO, as represented by the dominant EOFs of tropical Pacific SST

is a bit too limited compared to the observed pattern. There is very little difference between the patterns of three simulated first modes. For the second mode (middle row), a centre of high SST variability is located in the eastern equatorial Pacific, which is surrounded by opposite or out-of-phase variability of a horseshoe shape. The models more or less follow the observed pattern, but there are differences in detail. The third mode (bottom row) features a prominent variability centre in the central equatorial Pacific, with opposite variability elsewhere in the tropical Pacific. The models show a similar feature, but this is located to the north of the equator, is weak and accompanied by a second centre to the farther north. While the first mode has been used traditionally, the roles of additional modes have been emphasised recently for a more complete description of ENSO (Chattopadhyay et al., 2019; Timmermann et al., 2018). Despite the model biases discussed above, which are common to many state-of-the-art climate models, ACCESS-CM2 performs reasonably well in simulating the spatial structure of ENSO.

The ENSO events show considerable temporal variations in their structure and strength. One way of depicting these evolutions is by using one or more ENSO indices that are calculated from area-averaged SST anomalies over parts of the Tropical Pacific. A frequently used ENSO index is the Niño 3.4 index, which is calculated from SSTs over the central and eastern equatorial Pacific region: 5N–5S, 170W–120W. Here, we use this index to illustrate some of the salient temporal features (e.g., seasonality, characteristic time scales and the SST-thermocline depth relationship) of observed and simulated ENSO events. The ENSO-driven SST variability shows a pronounced annual variation, with the observed annual minimum occurring in May-June and the maximum in December-January (black curve in Fig. 5, left panel). This is true for the Niño 3.4 region (defined above); for other regions of the Tropical Pacific, the months of maximum and minimum SST variability may differ slightly. ENSO events typically start in April–June, hence the SST anomalies are weakest during these months.

The anomalies then grow during the subsequent months and reach their maximum amplitudes in December or January, after which they start to decay. The frequent occurrence of mature ENSO events during the Northern Hemisphere winter season, as implied by this figure, is often referred to as the seasonal phase locking of ENSO (Rashid & Hirst, 2016a). The model-simulated ENSO events in general show a similar annual variation, except that the SST variances tend to be stronger than observed during the earlier and later months of the calendar year (coloured curves in Fig. 5, left panel).

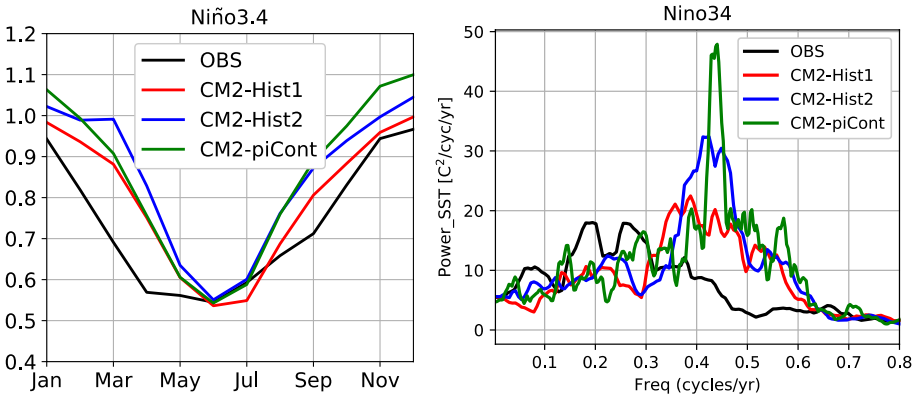

Figure 5. Annual variations of the standard deviations of ENSO-related SST anomalies (in degrees Celsius, left panel), and the power spectra (right panel) for observation (black curve) and model simulations (coloured curves).

ENSOs events occur once every of 2-8 years in observations, without showing a regular period. The characteristic timescale of ENSO may be demonstrated by a power spectrum analysis. The right panel of Fig. 5 shows the power spectra of the Niño 3.4 index computed from observation (black curve) and three ACCESS-CM2 simulations (coloured curves). The observed power (or variance) is weak at the very low and high frequencies, with two maxima occurring at around 6- and 4-year periods. The simulated spectra also show weak variances at the very low and high frequencies, as for the observed spectrum, but the maximum variance in this case occurs at higher frequencies (around 2.5 years) than in observation. In other words, the simulated ENSO events occur too frequently compared with the observed events. Note that there are some differences among the three simulations in the magnitude and the frequency of maximum power, but these differences are not as large as their differences with the observed spectrum. Similar higher-than-observed ENSO frequency is also seen in different segments of the pre-industrial control spin-up runs shown by Bi et al. (2020).

The quasi-biennial time evolution of the modelled ENSO events is a model deficiency that needs to be understood and, possibly, remedied. Some insights may be had by focusing on the elements of the ENSO feedback loop mentioned before: weaker easterly trade winds leading to smaller east-west SST gradients across the Pacific (and deeper thermocline in the eastern Pacific); in turn, the smaller SST gradient leads to weaker easterly winds. An important element of this feedback loop is the interaction between eastern Pacific SSTs and the zonally-averaged thermocline depth. To quantify the linear aspect of this interaction, we present in Fig. 6 the lead-lag correlations between the Niño-3 SST index and the Niño-3.4 D20 index for observation (black curve) and the three model simulations (coloured curves). We see that, at positive lags (i.e., when SST anomalies lead), the SST-D20 correlation values are similar in the observation and model

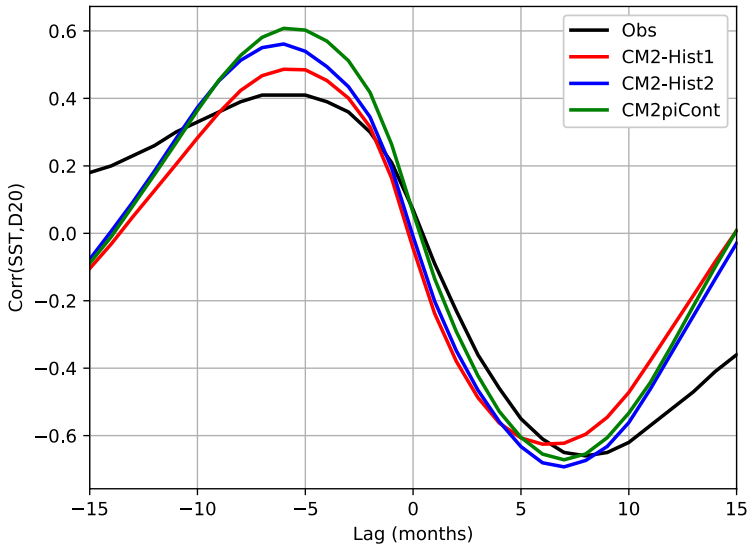

Figure 6. Cross correlations between the Niño-3 SST index and the Niño-3.4 D20 index as a function of time lag. The SST index leads at positive lags and the D20 index leads at negative lags. The Niño-3.4 D20 index is used as a proxy for zonally averaged thermocline depth anomalies, which in turn are an indication of the upper-ocean heat content in the tropical Pacific.

simulations, except that the maximum (negative) correlations occur somewhat earlier in simulations than in observation. At negative lags (when D20 anomalies lead), however, the simulated correlations are stronger than the observed, although the maximum values occur at about the same (negative) lag. This stronger than observed D20 forcing of ENSO-related SSTs, combined with the somewhat quicker response of D20 anomalies to the SST forcing, may contribute to the higher frequencies of the modelled ENSO events. Further investigation is, however, needed to draw a clearer conclusion about the mechanism of this ACCESS-CM2 model deficiency.

2.3 Rainfall simulation by a higher-resolution ACCESS-AM

Increasing the model resolution and improving model physics are the two main ways of improving the model simulations. In this section, we aim to understand the different mechanisms associated with the improvements seen from these two methods, as well as their limitations. Recommendations based on the model evaluations over the associated region of the Australian climate will be valuable contribution for future model development.

As mentioned earlier, three AMIP-style simulaitons with ACCESS-AM (the atmospheric component of ACCESS-CM2) were conducted. The first experiment was done with the same atmospheric model physics and horizontal resolution (~135 km) as in ACCESS-CM2 and this serves as the control experiment. In the second experiment, the horizontal resolution was increased by reducing the grid-spacing to ~60 km, to examine the effects of the increased resolution on rainfall simulation. The third experiment implements a simple prognostic based convective entrainment rate in the control experiment, which is expected to improve the tropical rainfall simulation. Figure 7 shows the averaged rainfall rate of the control experiment (Fig. 7a) and its averaged rainfall bias with respect to Global Precipitation Climatology Project observation (Fig. 7b). The results indicate that this version of ACCESS-AM has deficient rainfall (or dry biases) over the Maritime Continent

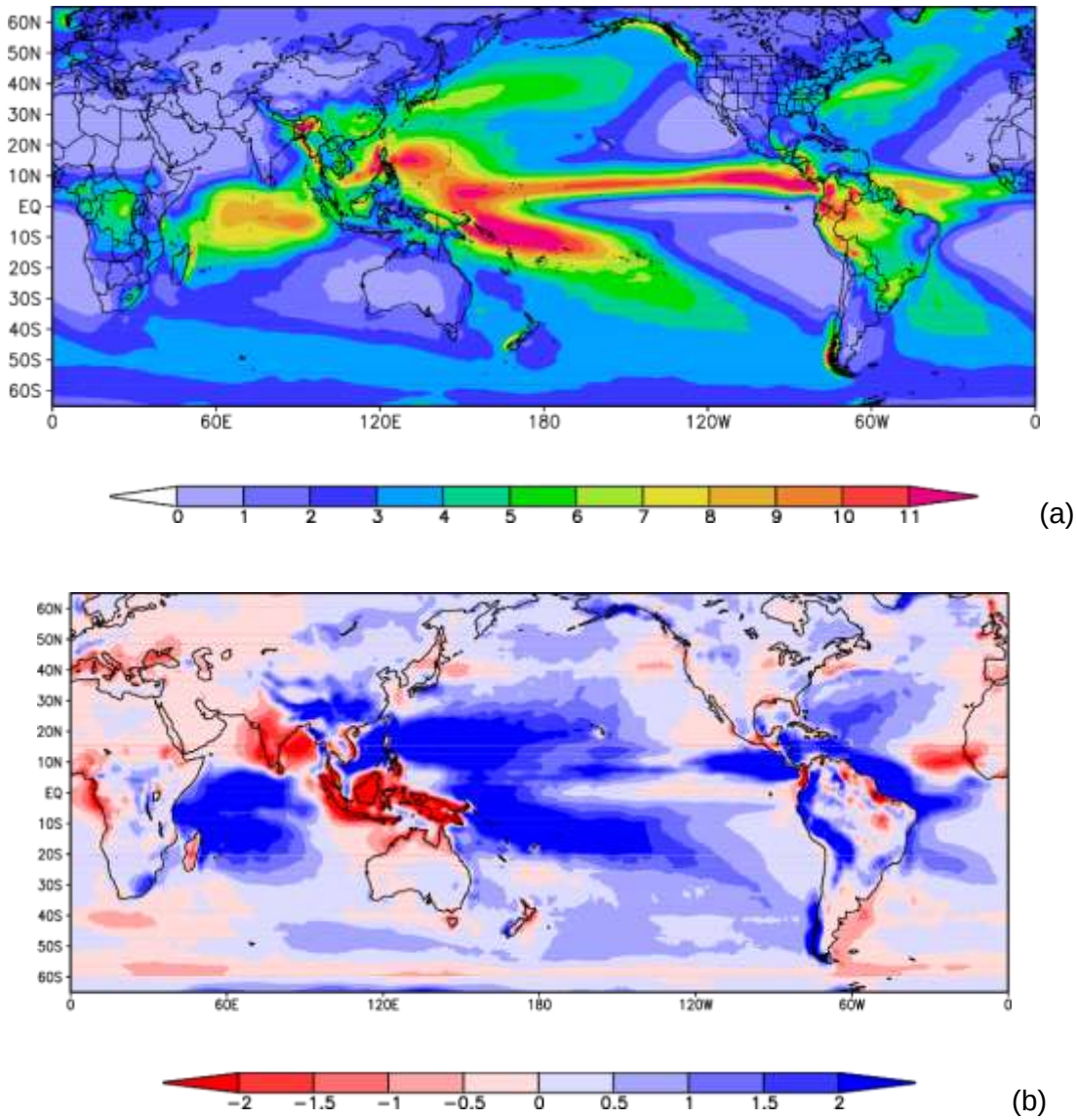

Figure 7. (a) Annual mean rainfall rate in mm/day for the ACCESS-AM control experiment; (b) Annual mean rainfall bias (mm/day) with respect to the GPCP rainfall observations (1989-2014).

region, the Indian subcontinent and northern Australia, as well as some other remote regions. However, the wet biases are spread over much of the tropical oceanic regions, with the largest biases seen over the western Indian Ocean and the western Pacific regions on both sides of the equator. These dry and wet rainfall biases have been a persistent issue in different versions of the ACCESS atmospheric model (Rashid & Hirst, 2016; Zhu et al., 2017).

The second experiment, carried out using a higher horizontal resolution (~60km) than the control experiment, shows an improvement in rainfall simulation. The difference of the annual mean rainfall rates between this experiment and the control experiment is shown in Fig.8. Due to the increased horizontal resolution in the model, the dry biases over the Maritime Continent and northern Australia are reduced. Consistent with this, the wet biases over the western Indian Ocean and the western Pacific are also reduced through the impacts of the Walker circulation. The wet biases near the northwest coast of South America are also reduced, but those in the ITCZ (the Inter-tropical Convergence Zone near the equatorial Pacific) get worse. Over the main part of Australia, the biases get worse with an increased dry bias to the west part and wet bias to the east part.

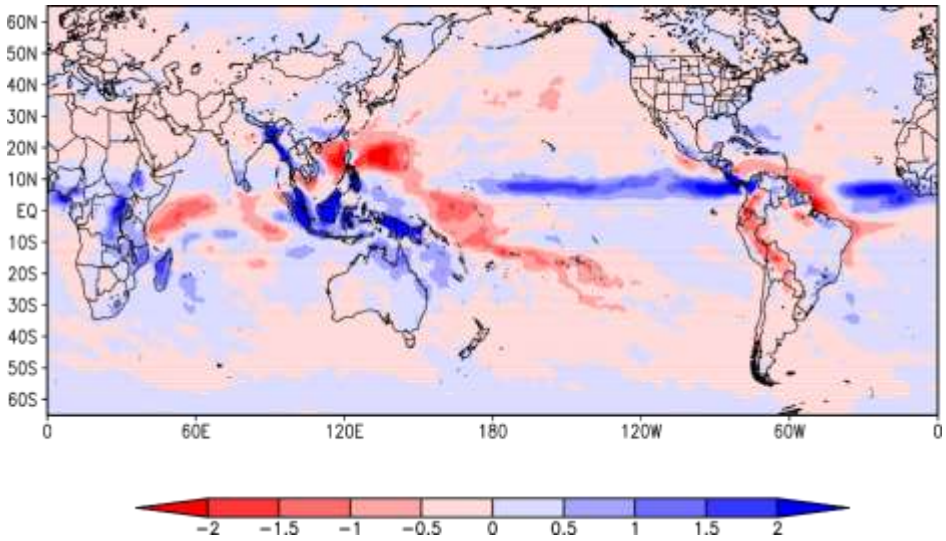

Figure 8. The difference of the annual mean rainfall rates (mm/day) between the experiment with 60 km resolution and the control experiment (135 km) for 1989-2014.

The third experiment uses the same model used for the control experiment, but with an updated convection scheme in which a simple prognostic based convective entrainment rate was implemented. The updated convection scheme will be included in the next version of ACCESS-AM, which is due to be released later this year (by the UK Met Office). The differences of the annual mean rainfall rates between the third experiment and the control experiment are shown in Fig. 9. With the improved convection scheme, the dry biases over the Maritime Continent and the north Australia are again reduced. This improvement is similar to, though not as large as, that resulted from increasing the horizontal resolution (Fig. 8). The wet biases over the western Indian Ocean and the northwest Pacific regions are also reduced. Unlike for the second experiment, however, the wet bias over the ITCZ has got smaller. There is a slight worsening of the dry bias over the south-eastern Indian Ocean. The biases over the main part of Australia have been improved.

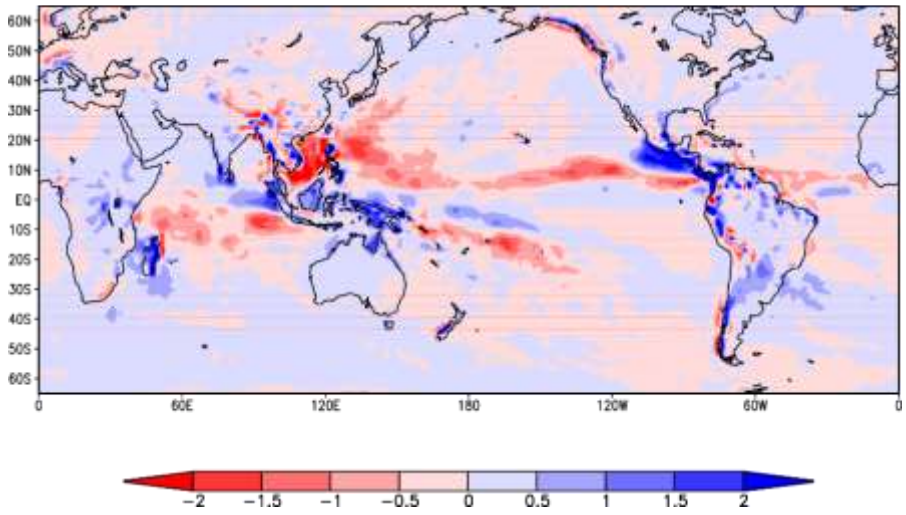

Figure 9. The difference of the annual mean rainfall rates (mm/day) between the model experiment with improved convection scheme and the control experiment. (1989-2014).

With an increased model horizontal resolution (second experiment) and an improved model physics (third experiment), the rainfall biases in ACCESS-AM simulations have improved over the tropical Indo-Pacific region. The rainfall bias over the ITCZ deteriorates with increasing horizontal resolution but has been seen to improve with the updated convection scheme. This suggests that the two model improvements affect the simulated rainfall and convection differently. In future work, we will do more evaluation in the areas of Monsoon, ENSO, seasonal rainfall biases over Australia, etc. New experiments with the latest UM (code version 11.4) will also be compared. Further investigations with ACCESS-AM will be conducted to better understand these different mechanisms. These studies are expected to provide guidelines for ACCESS climate modelling design and future ACCESS model development effort.

3 Conclusions

In this report, we have investigated the performance of ACCESS-CM2 and ACCESS-ESM1.5 in simulating some key features of historical climate. We have briefly examined the GMST simulations for up to year 2100, projected under the various CMIP6 future emission scenarios. Climate simulations from these two models have been contributed to the CMIP6 archive; analyses of these simulations and those from other climate models will feed into the upcoming IPCC AR6 report (Intergovernmental Panel on Climate Change Assessment Report 6). Since the initial submission to CMIP6, additional ensemble members have been generated from the two models, which have also been submitted to the CMIP6 archive. This report describes the result of preliminary analyses of the ensemble simulations from the two ACCESS models.

The ensemble-mean GMST simulations for the historical period follow closely the observed GMST, giving confidence to the ACCESS models' future projections. It is noted, however, that the simulated GMSTs are somewhat warmer than the observed, especially for ACCESS-ESM1.5. In this model, the warmer than observed SSTs appear to contribute to the warmer GMSTs simulated over the historical period. Warmer than observed SSTs are also simulated in ACCESS-CM2, but these are mainly over the Southern Ocean. In the Northern Hemisphere oceans, the SSTs are mostly cooler than observed, which partly compensate for the warm Southern Hemisphere SSTs. As a result, the historical GMST for this model is closer to the observed than for ACCESS-ESM1.5. For future projections, however, ACCESS-CM2 projects a warmer GMST at year 2100 (up to 6 degrees warmer than present days) than ACCESS-ESM1.5 does. This is because ACCESS-CM2 shows a higher climate sensitivity, the reasons for which are yet to be investigated. It should be noted that most CMIP6 climate models show higher climate sensitivities than the CMIP5 models (Zelinka et al., 2020).

The performance of ACCESS-CM2 in simulating the most important interannual climate variability mode (i.e., ENSO) has also been examined. Overall, the model does a good job in simulating the key features of ENSO. The tropical Pacific time-mean state and ENSO's spatial structure and seasonality are reasonably well simulated, although some biases are also identified. The prominent biases in the tropical time-mean state (which affects ENSO simulation) are cold SST bias, weak trade wind bias and shallow thermocline bias. The

main biases in ENSO properties are a somewhat meridionally confined spatial structure and an overly active and quasi-biennial ENSO. There are some differences among the three model simulations analysed, due to internal chaotic variability of the coupled ocean-atmosphere system. ENSO has a great influence on Australian (and global) weather and climate variability. It is therefore important to continue the effort to improve its simulation in the ACCESS model.

Some results from three AMIP (i.e., atmosphere-only) simulations are also presented. The main findings are: 1) due to an increased horizontal resolution, achieved by reducing the model's grid spacing from ~135 km to 60 km, the rainfall simulation is improved in many places, although the rainfall bias over the ITCZ is worsened and 2) a similar improvement is also obtained by implementing an updated convection scheme in the low-resolution atmospheric model. In this second case, however, the rainfall bias near the ITCZ also improves. This has implications for managing computational costs of climate models, given that models with higher resolutions are considerably more expensive than their lower-resolution counterparts.

The above preliminary analyses will be followed by a more comprehensive analysis of the ACCESS ensemble simulations in the coming months. This is expected to provide a more complete picture of ACCESS models' efficacy in simulating the historical climate, as well as a better estimate of future climate change. In addition, considerable time will be spent in articulating the value of ACCESS ensemble simulations for next-users (e.g., other ESCC Hub projects) and end-users or stakeholders. This will form the basis of the project-level synthesis report and also feed into the Hub level synthesis report.

4 Acknowledgements

We acknowledge all members of the ACCESS model development team for their contributions in developing and running the models and pre-processing and managing the output data. This work has been undertaken with funding from the National Environmental Science Program (NESP) Earth System and Climate Change (ESCC) Hub.

5 References

Bi D, Dix M, Marsland SJ, O'Farrell S, Sullivan A, Bodman R, Law R, Harman I, Srbinovsky J, Rashid HR, Dobrohotoff P, Mackallah C, Yan H, Hirst AC, Savita A, Boeira Dias F, Woodhouse M, Fiedler R, Heerdegen A. 2019. Configuration and spin-up of ACCESS-CM2, the new generation Australian Community Climate and Earth System Simulator Coupled Model, *Journal of Southern Hemisphere Earth Systems Science (JSHESS)*, accepted.

Bodman RW, Karoly DJ, Dix MR, Harman IN, Srbinovsky J, Dobrohotoff PB and Mackallah C. 2019. Evaluation of CMIP6 AMIP climate simulations with the ACCESS-AM2 model. *Journal of Southern Hemisphere Earth Systems Science (JSHESS),* in press.

Chattopadhyay R, Dixit SA, Goswami BN. 2019. A Modal Rendition of ENSO Diversity, *Scientific Reports*, doi: https://doi.org/10.1038/s41598-019-50409-4

Dee DP, Uppala SM, Simmons AJ, Berrisford P, Poli P, Kobayashi S, et al.(2011. The ERA-Interim reanalysis: configuration and performance of the data assimilation system, *Quarterly Journal of the Royal Meteorological Society*, 137(656), 553–597, doi: https://doi.org/10.1002/qj.828

Eyring V, Bony S, Meehl GA, Senior CA, Stevens B, Stouffer RJ, Taylor K E, 2016, Overview of the Coupled Model Intercomparison Project Phase 6 (CMIP6) experimental design and organization, *Geoscientific Model Development,* doi: https://doi.org/10.5194/gmd-9-1937-2016

Gates WL, Boyle JS, Covey C, Dease CG, Doutriaux CM, Drach RS, et al., 1999. An Overview of the Results of the Atmospheric Model Intercomparison Project (AMIP I), *Bulletin of the American Meteorological Society*, doi: https://doi.org/10.1175/1520-0477(1999)080<0029:AOOTRO>2.0.CO;2

Kosaka Y, Xie SP, 2013. Recent global-warming hiatus tied to equatorial Pacific surface cooling, *Nature*, 501, 403–407, doi: https://doi.org/10.1038/nature12534

Rashid HA, & Hirst AC, 2016a. Investigating the mechanisms of seasonal ENSO phase locking bias in the ACCESS coupled model. *Climate Dynamics*, 46, 1075–1090, doi: https://doi.org/10.1007/s00382-015-2633-y

Rashid HA, & Hirst AC, 2016b. Mechanisms of improved rainfall simulation over the Maritime Continent due to increased horizontal resolution in an AGCM, *Climate Dynamics*, 49, 1747–1764, doi:10.1007/s00382-016-3413-z

Rashid HA, Sullivan A, Hirst AC, Bi D, Zhou X, Marsland SJ. 2013. Evaluation of El Niño–Southern Oscillation in the ACCESS coupled model simulations for CMIP5. *Australian Meteorological and Oceanographic Journal*, 63, 161–180.

Rayner NA, Parker DE, Horton EB, Folland CK, Alexander LV, Rowell DP, et al., 2003. Global analyses of sea surface temperature, sea ice, and night marine air temperature since the late Nineteenth Century, *Journal of Geophysical Research*, 108 (4407), doi: https://doi.org/10.1029/2002JD002670

Risbey JS, Lewandowsky S, Langlais C, Monselesan DP, O'Kane TJ., Oreskes N, 2014. Well-estimated global surface warming in climate projections selected for ENSO phase *Nature Climate Change*, doi: https://doi.org/10.1038/nclimate2310

Timmermann A, An S, Kug J, Jin F, Cai W, Capotondi A, Cobb K, Lengaigne M, McPhaden MJ, Stuecker MF, Stein K, Wittenberg AT, Yun K, Bayr T, Chen H, Chikamoto Y, Dewitte B, Dommenget D, Grothe P, Guilyardi E, Ham Y, Hayashi M, Ineson S, Kang D, Kim S, Kim W, Lee J, Li T, Luo J, McGregor S, Planton Y, Power SB, Rashid H, Ren H, Santoso A, Takahashi K, Todd A, Wang GM, Wang GJ, Xie R, Yang H, Yeh S, Yoon J, Zeller E, Zhang X. 2018. El Niño–Southern Oscillation complexity, *Nature,* 559, 535-545, doi: https://doi.org/10.1038/s41586-018-0252-6

Uppala SM, KÅllberg PW., Simmons AJ, Andrae U, Bechtold VDC, Fiorino, M, et al., 2005. The ERA-40 re-analysis, *Quarterly Journal of the Royal Meteorological Society*, 131(612), 2961–3012, doi: https://doi.org/10.1256/qj.04.176

Walters D, Baran AJ, Boutle I, Brooks M, Earnshaw P, Edwards J, et al., 2019. The Met Office Unified Model Global Atmosphere 7.0/7.1 and JULES Global Land 7.0 configurations, *Geoscientific Model Development*, 12(5), 1909–1963, doi: https://doi.org/10.5194/gmd-12-1909-2019

Wilcox LJ, Highwood EJ, Dunstone NJ. 2013. The influence of anthropogenic aerosol on multi-decadal variations of historical global climate, *Environmental Research Letters*, doi: https://doi.org/10.1088/1748-9326/8/2/024033

Yin Y, Alves O, Oke PR. 2011. An Ensemble Ocean Data Assimilation System for Seasonal Prediction, *Monthly Weather Review,* 139(3), 786–808, doi: https://doi.org/10.1175/2010mwr3419.1

Zelinka MD, Myers TA, McCoy DT, Po-Chedley S, Caldwell PM, Ceppi P, et al. 2020. Causes of Higher Climate Sensitivity in CMIP6 Models, *Geophysical Research Letters,* doi: https://doi.org/10.1029/2019GL085782

Zhu HY, Maloney E, Hendon H, Stratton R. 2017. Effects of the changing heating profile associated with melting layers in a climate model, *Quarterly Journal of the Royal Meteorological Society*, 143, 3110-3121, doi:10.1002/qj.3166

Ziehn T, Chamberlain M, Law R, Lenton A, Bodman R, Dix M, Stevens L, Wang YP, Srbinovsky. 2020. The Australian Earth System Model: ACCESS-ESM1.5*. Journal of Southern Hemisphere Earth Systems Science (JSHESS)*, accepted

Earth Systems and Climate Change Hub

National Environmental Science Programme

www.nespclimate.com.au